International Journal of Multiphase Flow 37 (2011) 1–11

Contents lists available at ScienceDirect

International Journal of Multiphase Flow

journal homepage: www.elsevier.com/locate/ijmulflow

Trapped water displacement from low sections of oil pipelines

Guang-li Xu [a,b], Guo-zhong Zhang [a], Gang Liu [a], Amos Ullmann [b], Neima Brauner [b,*]

[a] College of Pipeline and Civil Engineering, China University of Petroleum, Qingdao 266555, China
[b] School of Mechanical Engineering, Tel Aviv University, Tel Aviv 69978, Israel

ARTICLE INFO

Article history:
Received 9 May 2010
Received in revised form 6 September 2010
Accepted 6 September 2010
Available online 17 September 2010

Keywords:
Oil–water flow
Water displacement
Inclined pipe
Water plug
Pipeline corrosion

ABSTRACT

The study is motivated by the problem of pipeline corrosion due to water accumulation at low spots. Lab-scale experiments were conducted to identify the critical conditions required for the onset of water displacement by oil flow from a low horizontal section into an upward inclined section of the pipeline. Two test loops with pipe diameters of 27 mm and 41 mm I.D. with diesel flow were used. Water withdrawal from tapping valves distributed along the up-hill section enabled to follow the water displacement for oil flow rates exceeding the critical value.

A model for predicting the water displacement by the oil flow, which is based on the formation of a water plug in the lowest (horizontal) section, is suggested. The predicted amounts of water withdrawn from the tapping valves favorably compare with the experimental results. Considering other competing mechanisms, up-scaling to larger pipe diameters is examined. The analysis indicates that water plug formation appears to be the controlling mechanism for water displacement also in larger pipe diameters encountered in field operations.

© 2010 Elsevier Ltd. All rights reserved.

1. Introduction

Maintenance of oil pipelines to avoid leakage or blockage of the flow is of a major concern to the oil companies. These may be caused by corrosion of the pipe in the presence of water. The resulting wall-deposited products increase the pipe wearing. When carried by the oil flow, they can plug the pipe line equipment (e.g., filters, valves, pumps). For example, pipeline blockage caused by corrosion sediments had happened many times in China (Tao et al., 2006). The sediments main constituent was found to be iron oxide (Fe_2O_3) (Yang, 2009), as a result of some left-over water introduced during water tests, which tend to accumulate at low level locations along the pipe line. The unplanned shut-down accidents may have a great bad impact on the regular oil transportation plan. For example, when heavy contaminated oil has been pumped to a higher elevation and followed by lighter and cleaner oil, unplanned shut-down accident results in unwanted mixing and the formation of a large volume of low quality oil. In natural gas pipelines, the presence of water may result in the formation of gas hydrates during shutdown, which can plug pipeline and process equipment. Flushing out of the water from the pipe by the oil flow is required to avoid those damages and shut-down accidents in oil pipelines, and can be considered also as one of the options to avoid the hydrate formation in natural gas pipelines. From a practical point of view, the minimal oil flow rate required for displacement of the accumulated water by the oil flow has to be determined.

Industrial pipelines consist of horizontal, up-hill and downhill sections. Hence, the prediction of the water displacement by the oil flow requires the modeling of oil–water flow in hilly terrain pipelines under transient and steady conditions. Most of the literature on oil–water flow refers to flow patterns, holdup and pressure gradient for specified oil and water flow rates and a constant pipe inclination. A review of the literature on experimental studies and modeling of oil–water two-phase flow systems is presented in Brauner (e.g., 1998, 2003). Two main procedures were used for introducing the oil and water into the test section: pumping water and oil separately and mixing them in a T or Y junction (e.g., Lovick and Angeli, 2004; Rodriguez and Oliemans, 2006; Chakrabarti et al., 2007), or introducing an oil–water dispersion formed in a pre-mixing tank (e.g., Chen et al., 2001, 2003; Arirachakaran et al., 1989; Shi et al., 2003). The results of such studies are not applicable for predicting the water displacement and other flow characteristics in the case of water trapped by the oil flow in hilly terrain pipelines, where the water flow rate and holdup are unknown.

In this study lab-scale experiments were conducted to identify the critical conditions required for the onset of the displacement of water trapped in a low section of a pipeline and subsequently carried by the oil flow into an up-hill section of a pipe. Water withdrawal from tapping valves distributed along the up-hill section enabled to follow the water displacement for oil flow rates exceeding the critical value. The experimental setup and the results are

* Corresponding author. Tel.: +972 3 640 3127; fax: +972 3 640 7334.
E-mail address: brauner@eng.tau.ac.il (N. Brauner).

0301-9322/$ - see front matter © 2010 Elsevier Ltd. All rights reserved.
doi:10.1016/j.ijmultiphaseflow.2010.09.003

described in Sections 2 and 3 respectively. A model for predicting the onset of water displacement and the resulting oil–water two-phase flow in the up-hill section is presented (Section 4) and compared with the experimental results (Section 5). Finally, the underlying mechanisms and scale-up to large pipe diameters are discussed (Section 6).

2. Experimental system

Diesel and tap water were used as test liquids. The water and oil physical properties at room temperature are listed in Table 1. The experimental studies on water displacement by the oil flow were performed in the flow system which is schematically described in Fig. 1a.

Oil is pumped from its reservoir through a set of calibrated flowmeter with an accuracy of ±1% into the test section, and is collected back in the storage tank. The test section shown in Fig. 1b consists of 3° downward, horizontal and 12° upward sections, with length of 1-m, half-m and 4-m respectively. Water is injected into the bottom of the horizontal test section. The experiments were conducted in two sets of steel pipes of 27 mm and 41 mm diameters (I.D.). To enable measurement of water amount carried by the oil flow, 6 mm tapping points equipped with ball valves are distributed along the bottom of the upward inclined test section. In the 27 mm pipe there are four tapping valves (Nos. 1–4, see Fig. 1), which are located at 0.5 m, 1.5 m, 2.5 m and 3.5 m downstream the end of the horizontal section. In the 41 mm pipe, only three tapping valves were installed (Nos. 2–4). The system is mounted on a support system, which provides space to empty the entire flow loop through an outlet (No. 0) placed on the horizontal test section at the lowest part of the loop.

Water is injected into the bottom of the horizontal test section using an in-house injection setup which is shown in Fig. 1c. It consists of a 3.7 mm I.D. metal tube, one of its ends ('1') is plugged to the bottom of the horizontal test section through a nozzle (welded on the horizontal test section, '2') and a ball valve ('3'). The other end of the metal tube is connected to the injector through a rubber sealing hose ('4').

The instrumentation used in the experiments provided three types of data: the pressure drop, the flow rate of oil and the water volume carried out by the oil. The pressure drop was recorded using a differential pressure transducer (EJA1110A, with an accuracy of 30 Pa) with tapping ports (flanges) located 6 m apart at the two ends of the test section. The flow rate of oil was recorded using a flow transmitter (LWGY-1540, with an accuracy of 0.02 m^3/h). At the beginning of the tests, the transducer and the flow transmitter were calibrated. The volume of the displaced water that flowed through an opened tapping point (Nos. 1, 2, 3 or 4) in the time period of 5 min was measured by a volumetric cylinder. The No. 0 outlet was used to measure the volume of water which did not reach the tapping point and therefore was left in the system.

A needle valve and a by-pass were used to control the oil flow rate. In order to avoid the influence of vibration of the magnetic centrifugal pump on water displacement and withdrawal, two hoses were installed at both the inlet and outlet of the pump. The temperature change of the diesel was recorded by a temperature sensor installed in the oil tank and was found to be less than 5 °C during an experiment, so the impact of temperature variation on the physical properties can be considered negligible.

Table 1
Properties of diesel and water at 25 °C.

Fluids	Diesel	Tap water
Density (kg/m^3)	855.83	997.04
Viscosity (mPa s)	3.43	0.895
Interfacial tension (mN/m)	18.33	

The range of oil flow rate tested is 0.16–0.49 m^3/h for the system with the 27 mm diameter pipe and 0.58–0.91 m^3/h for the system with the 41 mm diameter pipe, respectively. The maximal oil flow rate corresponds to Reynolds number less than 2000, hence all data correspond to laminar oil flow. The volume of water injected into horizontal section was set to 15, 25 and 40 ml.

At the beginning of each experimental run, oil was pumped through the system at the highest flow rate to remove the air. Then, the oil flow rate was adjusted to the desired value, the pump was stopped and the water injector was carefully connected to the bottom of the horizontal test section. Upon completing the process of water injection, the pump was re-started and simultaneously one of the outlet taps along the upward inclined section was opened for a constant time period of 5-min to measure the volume of water withdrawn during this time. Then, the pump was stopped and simultaneously the valve was closed, and the entire flow loop was emptied through No. 0 outlet. The volume of water remained in the entire loop was measured to confirm the water mass balance. The experimental error in the water volume measurements is ±2%. This procedure was repeated for each of the tapping valves. The data can be used also to estimate the distance over which the water was carried by the oil during the 5 min time period (see below). Note that the sampling time period does not correspond to time during which the water were actually collected in the volumetric cylinder, and therefore, the data cannot be used to estimate the average water flow rate (Q_w) through the upward inclined section.

Tests were repeated to check the repeatability and to estimate the experimental error in the data of water withdrawn volume. The reported error is taken as the root mean square error (RMSE) of repeated measurements, with a minimum of 20%.

3. Experimental results

The measured volume of water withdrawn during 5 min from the different tapping valves vs. the oil superficial velocity is shown in Figs. 2 and 3 for the D = 27 mm and D = 41 mm pipes, respectively. The results shown are for three different amounts of injected water, V_w = 15, 25 and 40 ml. The results indicate the existence of a minimal flow rate for the onset of water displacement by the oil flow that enables their withdrawal downstream the horizontal section. The curves shown in these figures are the prediction of the model presented below (Section 4).

Comparison of Figs. 2 and 3 implies that for the same volume of injected water the critical oil superficial velocity increases with the pipe diameter. With U_{os} exceeding the critical velocity, there is an abrupt increase in the amount of water withdrawn. The results also indicate that larger superficial oil velocities are required to withdraw the water from tapping points located further downstream the upward inclined pipe. These results can be used to estimate the water propagation velocity in the upward inclined pipe for oil superficial velocities exceeding the critical value.

The experimental data yield also the value of U_{os} for which water flow through a tapping valve located at a distance l along the upward inclined section (0.5, 1.5, 2.5, 3.5 m) was first detected during the 5 min (t = 300 s) of the experiment. The corresponding water velocity $U_w = l/t$. This velocity vs. the oil superficial velocity is depicted in Fig. 4 for the two pipes used in the experiments. The results indicate an increase of U_w with U_{os}. The four data points for D = 27 mm system were fitted by linear model ($U_w = 0.17U_{os}–0.013$). Then, the three points in the 41 mm diameter system (corresponding to tapping valves at 1.5, 2.5, 3.5 m) were fitted with the same slope (0.17). As shown, a linear relationship results in a good fit with the

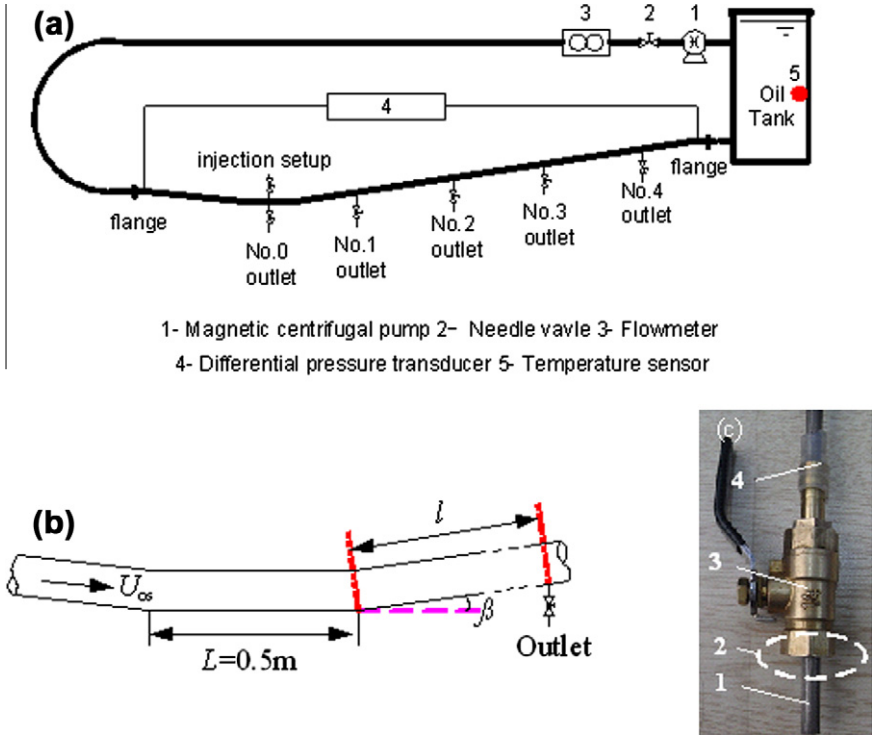

Fig. 1. Schematic description of the experimental setup: (a) the flow system; (b) test sections; (c) injection setup.

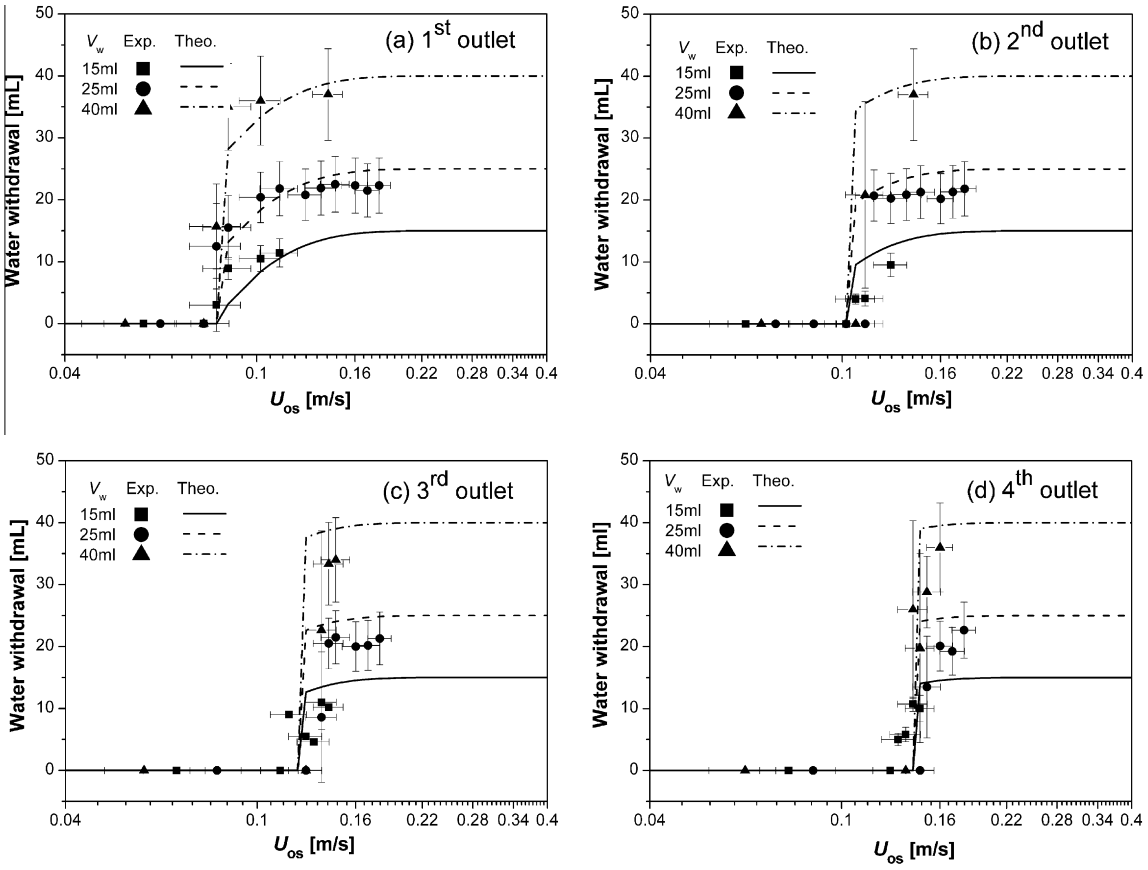

Fig. 2. Water withdrawal from four tapping valves vs. U_{os} for various amounts of water injection (V_w = 15, 25, 40 ml) in the D = 27 mm system: experimental results and model predictions.

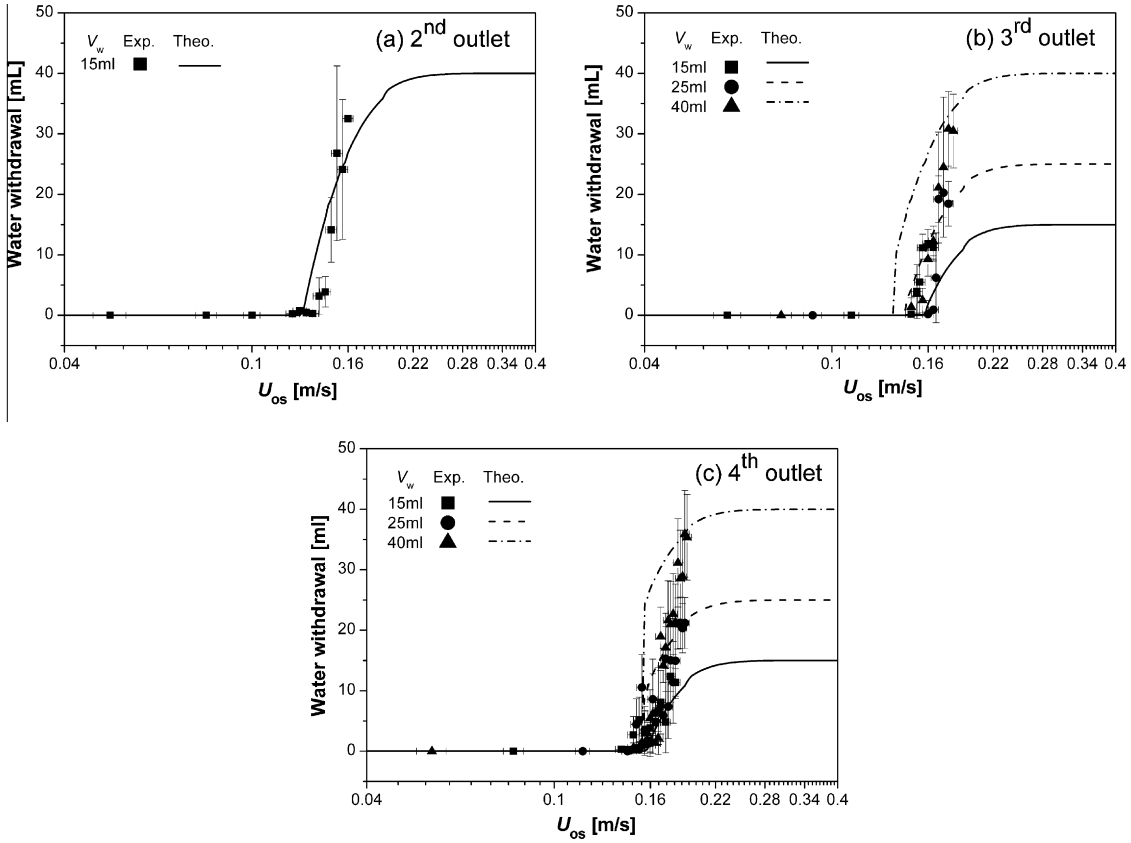

Fig. 3. Water withdrawal from three tapping valves vs. U_{os} for various amounts of water injection (V_w = 15, 25, 40 ml) in the D = 41 mm system: experimental results and model predictions.

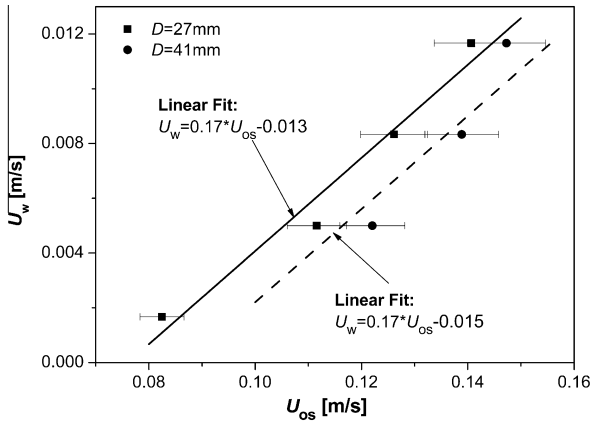

Fig. 4. The relationship between the water velocity and the superficial velocity of oil. The solid line represents the D = 27 mm system, while the dash line denotes the D = 41 mm system.

coefficient of determination (R^2) 0.966 for the D = 27 mm system and 0.858 for D = 41 mm system.

4. Modeling

The physical model refers to the water displacement by oil flow which has been studied in the flow loop described in Section 2. Three main mechanisms for water displacement out of the horizontal section by the oil flow can be considered:

- Instability of the oil–water interface which leads to water drop entrainment.
- Formation of a water plug which is pushed by the oil flow.
- Breakage of water into drops and the formation of water-in-oil dispersion.

The dispersion of water into drops requires turbulence in the oil flow, which is relevant for higher flow rates than those used in the experimental studies. Therefore hereunder, the two first mechanisms are considered.

4.1. Instability of the oil–water interface

A certain amount of stagnant water (V_w), is introduced into the lowest elbow (the horizontal section) of the flow loop. The water spreads over the length (L) of the horizontal section, resulting in an average water level, $\tilde{h}_{av}$, corresponding to an average holdup of $\varepsilon = V_w/(AL) = A_w/A$. For $U_o \gg U_w$ ($U_w \approx 0$) only the oil phase momentum equation may be considered, whereby the condition for Kelvin–Helmholtz (K–H) long-wave instability (e.g., Brauner and Moalem Maron, 1992) reads:

$$U_{os} \geqslant \sqrt{\frac{C(\rho_w - \rho_o)g\cos\beta A_o^3}{\pi^2 D^4 \rho_o \mathrm{d}A_w/\mathrm{d}h}} \tag{1.1}$$

The geometrical relationships for $\tilde{A}_{o,w} = A_{o,w}/D^2$ and $\mathrm{d}\tilde{A}_w/\mathrm{d}\tilde{h}$ are all expressed in terms of $\tilde{h} = h/D$:

$$\theta = \arccos(1-2\tilde{h}); \quad \tilde{A}_o = \frac{1}{4}\left[\pi - \theta + \frac{\sin(2\theta)}{2}\right];$$

$$\tilde{A}_w = \frac{1}{4}\left[\theta - \frac{\sin(2\theta)}{2}\right]$$

$$\mathrm{d}\tilde{A}_w/\mathrm{d}\tilde{h} = \sin\theta = -\mathrm{d}\tilde{A}_o/\mathrm{d}\tilde{h} \tag{1.2}$$

Table 2
The minimal superficial velocity of oil (critical U_{os} (m/s)) calculated by Eq. (1) with $C = 12$ (laminar flow) in the two systems for different water volumes.

	V_w (ml)		
D (mm)	40	25	15
27	0.14	0.17	0.19
41	0.23	0.25	0.28

The constant C in Eq. (1.1) is dependent on the velocity profile of the oil (represented by the velocity profile shape factor γ_o). For turbulent flow (i.e., plug flow can be assumed) $\gamma_o \approx 1$, $C = 16$, while with laminar (Poiseuille) profile $\gamma_o \approx 4/3$ and $C = 12$.

The resulting minimal (critical) U_{os} values required for the onset of interfacial instability are given in Table 2 for the various water amounts and the two pipe diameters used in the experiments. Comparison with the experimental results shown in Fig. 5 indicates that the critical U_{os} values predicted by Eq. (1) are much larger than the experimental U_{os} for which water displacement into the upward inclined section was detected. This implies that K–H instability of the water interface is not the dominating mechanism which sets the critical conditions for the onset of water displacement by the oil flow.

4.2. Water plug formation

Upon switching-on the oil flow, the volume (V_w) of water is redistributed in the horizontal section of the flow loop. The shear exerted by the oil on the water interface pushes the water towards the elbow and causes the water level to rise downstream. For a sufficiently large oil flow rate, a water plug can be formed, which is then pushed by the oil flow into the upward inclined pipe. It is assumed that the critical conditions for the onset of water displacement correspond to the minimal oil flow rate required for the formation of a water plug. The amount of water pushed into the inclined section may redistribute by the flow field upon propagating upward. The oil–water flow pattern in the upward inclined pipe determines the water propagation velocity. This in turn determines the amount of water that could reach the tapping valves which are distributed along the upward inclined pipe during the time frame of the experiment.

Accordingly, the water distribution in the horizontal section is modeled to determine the critical conditions for the formation of a water plug and the amount of water pushed into the upward inclined section. The model considers the final steady state water level profile and ignores the transient process that leads to its establishment.

4.2.1. Water level profile in the horizontal section

Consider water and oil layers in a horizontal tube of a length L. The flow configuration and coordinates are illustrated in Fig. 6. The oil flow drags the water, pushing it towards the wall at $x = L$. Consequently, the water level rises downstream.

Utilizing the average one-dimensional Two-Fluid model formulation and assuming steady conditions, the momentum equations of each of the fluids (simplified by the Leibnitz rule) read:

$$\rho_w U_w \frac{dU_w}{dx} = -\frac{\tau_w S_w}{A_w} + \frac{\tau_i S_i}{A_w} - \frac{dP_{iw}}{dx} - \rho_w g \frac{dh}{dx} \tag{2}$$

$$\rho_o U_o \frac{dU_o}{dx} = -\frac{\tau_o S_o}{A_o} - \frac{\tau_i S_i}{A_o} - \frac{dP_{io}}{dx} - \rho_o g \frac{dh}{dx} \tag{3}$$

where $A_{o,w}$ and $S_{o,w}$ are the cross-sectional area and the wall perimeter of each of the fluid, S_i is the interfacial perimeter, $P_{io,iw}$ are the pressure at the interface in two-phases, $U_{o,w}$ are the average local velocities and h is the water level. The velocity of the water is very low compared to the fast moving oil, hence $U_w \approx 0$ (and $\tau_w \approx 0$) can be assumed in the model. Ignoring also surface tension effects, $P_{io} \approx P_{iw}$, the combined momentum equation reads:

$$\rho_o U_o \frac{dU_o}{dx} = -\frac{\tau_o S_o}{A_o} - \frac{\tau_i S_i}{A_o} - \frac{\tau_i S_i}{A_w} + (\rho_w - \rho_o) g \frac{dh}{dx} \tag{4}$$

The oil mass conservation equation reads:

$$U_o A_o = Q_o = U_{os} A \tag{5}$$

or:

$$U_o = \frac{U_{os}}{1 - \varepsilon} \tag{6}$$

where $\varepsilon = A_w/A$ is the water holdup. Accordingly:

$$\frac{dU_o}{dx} = Q_o \frac{d}{dh}\left(\frac{1}{A_o}\right)\frac{dh}{dx} \tag{7}$$

Substituting Eq. (7) into Eq. (4) and using dimensionless variables (superscript $\sim$ denotes normalized variables, area by D^2 and length by D) results in:

$$\frac{d\tilde{h}}{d\tilde{x}} = \left[\frac{\tau_o \tilde{S}_o}{\tilde{A}_o} + \tau_i \tilde{S}_i \left(\frac{1}{\tilde{A}_o} + \frac{1}{\tilde{A}_w}\right)\right] \Big/ \left[\rho_o \frac{U_o^2}{\tilde{A}_o} \frac{d\tilde{A}_o}{d\tilde{h}} + (\rho_w - \rho_o) Dg\right] \tag{8}$$

The geometrical relationships are all expressed in terms of $\tilde{h}$ (see Eq. (1.2)) and $\tilde{S}_o = \pi - \theta$; $\tilde{S}_i = \sin\theta$.

As conventionally used in the Two-Fluid model, the wall and interfacial shear stresses τ_o and τ_i are expressed in terms of the corresponding friction factors. For $U_o \gg U_w$, $\tau_i \approx \tau_o$, whereby (Brauner and Moalem Maron, 1989):

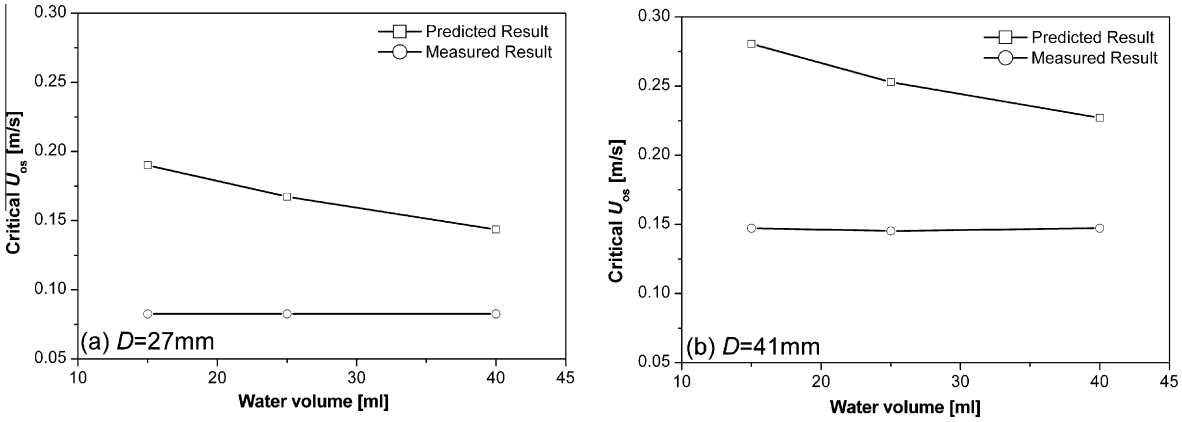

Fig. 5. Comparison of the critical U_{os} between the predicted value by Eq. (1) and the measured value.

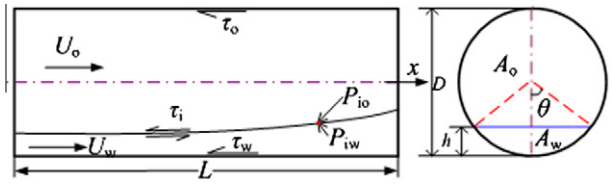

Fig. 6. Schematic description of oil–water stratified flows in horizontal tube.

$$\tau_o = \frac{1}{2}\rho_o f_o |U_o| U_o = \tau_i \tag{9}$$

$$f_o = \frac{c_o}{Re_o^{n_o}}; \quad Re_o = \frac{\rho_o |U_o| D_o}{\mu_o}; \quad \widetilde{D}_o = \frac{4\widetilde{A}_o}{\widetilde{S}_i + \widetilde{S}_o} \tag{10}$$

where $\widetilde{D}_o$ is the hydraulic diameter and c_o, n_o are adjusted according to the flow regime (e.g., laminar: $c_o = 16$, $n_o = 1$, turbulent: $c_o = 0.046$, $n_o = 0.2$).

Thus, the water level profile in the horizontal section can be obtained by numerical integration of Eq. (8) combined with Eq. (5) and Eqs. (9) and (10), the geometrical relations and the oil physical properties.

The numerical integration of Eq. (8) requires a value for initial water level $\tilde{h}^0$, and can be carried out to the critical point where the denominator of Eq. (8) vanishes, and $d\tilde{h}/dx \to \infty$ at $\tilde{h} = \tilde{h}_{cr}$. Downstream the critical point a water plug may be formed. Obviously, the feasible water level profile is constrained by the amount of water introduced into the horizontal section ($V_w < L\pi D^2/4$). Accordingly, depending on V_w and the oil flow rate, four different cases should be considered (see Fig. 7):

Case a:

$$\int_0^L A_w(h)dx = V_w; \quad \text{with } \tilde{h}^0 > 0 \text{ and } \tilde{h}|_{x=L} < \tilde{h}_{cr} \tag{11.1}$$

The oil superficial velocity is low, and although the water level rises downstream, a water plug is not formed and the entire length of the horizontal section remains wetted by the water ($L_{dry} = 0$).

Case b:

$$\int_0^{L_1} A_w(h)dx = V_w; \text{ with } L_1 < L, \text{ hence } \tilde{h}^0 = 0, \text{ but } \tilde{h}|_{x=L_1} < \tilde{h}_{cr} \tag{11.2}$$

In this case the water is pushed towards the elbow side wall, resulting in a dry zone length of $L_{dry} = L - L_1$. Yet, as $\tilde{h}|_{x=L_1} < \tilde{h}_{cr}$, a water plug is not formed.

Case c:

$$\int_0^{L_1} A_w(h)dx = V_{L_1} < V_w; \text{ with } L_1 + L_2 < L, \text{ hence } \tilde{h}^0 = 0, \text{ and } \tilde{h}|_{x=L_1} = \tilde{h}_{cr} \tag{11.3}$$

The water is pushed towards the elbow side wall, however as $\tilde{h}|_{x=L_1} = \tilde{h}_{cr}$ with $V_{L_1} < V_w$, a water plug is formed. The amount of water in the plug is $(V_w - V_{L_1})$, and its length is $L_2 = (V_w - V_{L_1})/A$, where L_1 is the length of the water plug tail. The length of the dry zone in this case is $L_{dry} = L - L_1 - L_2$.

Case d:

$$\int_0^{L_1} A_w(h)dx = V_{L_1} < V_w; \text{ with } L_1 + L_2 = L, \text{ hence } \tilde{h}^0 \geqslant 0, \text{ and } \tilde{h}|_{x=L_1} = \tilde{h}_{cr} \tag{11.4}$$

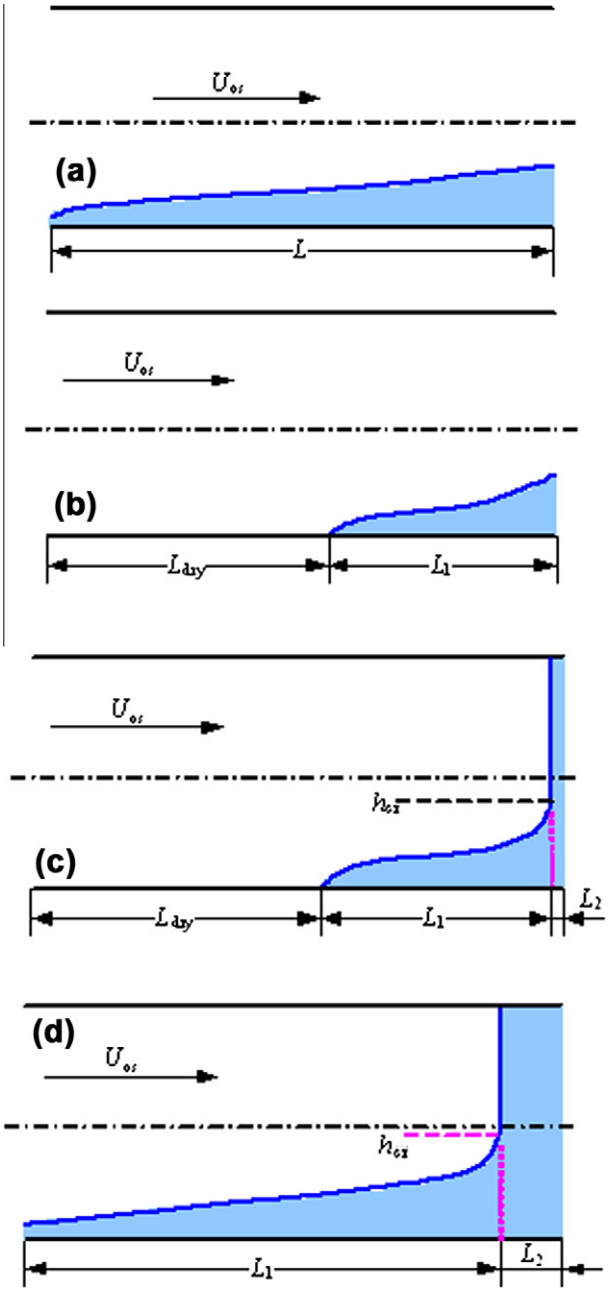

Fig. 7. Schematic description of the water level profile in the horizontal section: (a) water level rises downstream; (b) water is pushed towards the elbow but a plug is not formed; (c) water plug is formed with $\tilde{h}^0 = 0$; (d) water plug is formed with $\tilde{h}^0 > 0$.

In this case a plug is formed, and the entire lower section remains wetted by water. Assuming $\tilde{h}^0 = 0$, would result in $L_1 + L_2 \geqslant L$. If $L_1 + L_2 > L$, the solution is iterated to find a value of $\tilde{h}^0 > 0$, which satisfies the length constrain, $L_1 + L_2 = L$, as well as the water volume constrain, $V_{L_1} + (\pi D^2/4)L_2 = V_w$.

The critical water level $\tilde{h}_{cr}$ corresponds to the condition where the oil inertia is balanced by the gravitational term (in the denominator of Eq. (8)). It is obtained by the solution of the following equation:

$$\frac{4U_o^2 \cdot \sin[\arccos(1 - 2\tilde{h}_{cr})]}{\pi - \arccos(1 - 2\tilde{h}_{cr}) + \frac{1}{2}\sin[2\arccos(1 - 2\tilde{h}_{cr})]} = \frac{(\rho_w - \rho_o)Dg}{\rho_o} \tag{12}$$

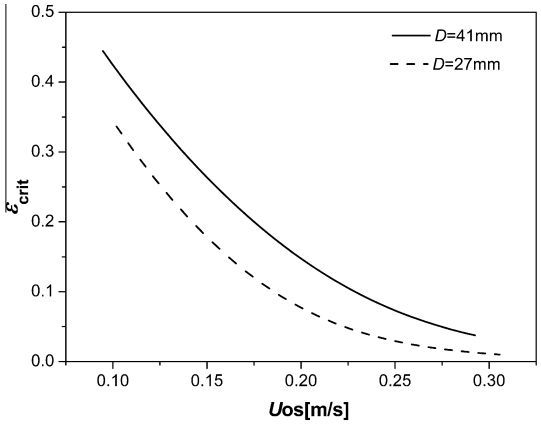

Fig. 8. The critical water holdup vs. the superficial velocity of oil for two systems.

Given the pipe diameter and the physical properties, the critical water level depends only on the superficial oil velocity. Fig. 8 demonstrates the effect of the superficial oil velocity and pipe diameter on the water holdup corresponding to $\tilde{h} = \tilde{h}_{cr}$. As shown in Fig. 8 the critical water holdup deceases with increasing U_{os}, hence a water plug may be formed with a smaller amount of water in the pipe. However, as the critical water holdup increases with increasing the pipe diameter, a higher U_{os} is required for the formation of a plug in a larger pipe diameter.

It is worth noting in cases *b* and *c*, the integration of Eq. (8) starts at $\tilde{h}^0 = 0$, where Eq. (8) reduces to:

$$\frac{d\tilde{h}}{d\tilde{x}} = \frac{\tau_{os}\tilde{S}_i}{\tilde{A}_w \Delta\rho g D} \tag{13}$$

where τ_{os} is the superficial wall shear stress of the oil for the case in which the oil wets the entire tube wall.

For $\tilde{h}^0 \to 0$, $\theta \to 0$, hence $\tilde{S}_i$, $\tilde{A}_w \to 0$, and both the numerator and denominator of Eq. (13) vanishes. The initial integration from $\tilde{h}^0 = 0$ to a finite small $\tilde{h}$ is taken analytically. Using Taylor's expansion shows that for $\tilde{h} \to 0$, $\tilde{A}_w = \theta^3/6$, $\tilde{h} = \theta^2/4$, $\tilde{S}_i = \theta$, whereby Eq. (13) reduces to:

$$\frac{d\tilde{h}}{d\tilde{x}} = \frac{3\tau_{os}}{2\Delta\rho g D\tilde{h}} \tag{14}$$

Whereby the nonzero boundary condition for the numerical integration is replaced by $\tilde{h}_{0N}$ at $\tilde{x} = \tilde{x}_{0N}$ given by:

$$\tilde{h}_{0N} = \sqrt{\frac{3\tau_{os}}{\Delta\rho g D}\tilde{x}_{0N}} \tag{15}$$

The corresponding water volume, V_{0N} (which should be added to the results of the numerical integration) is given by:

$$V_{0N} = \frac{2}{21}\left(\frac{48D^3\tau_{os}}{\Delta\rho g}\right)^{3/4}\tilde{x}_{0N}^{7/4} \tag{16}$$

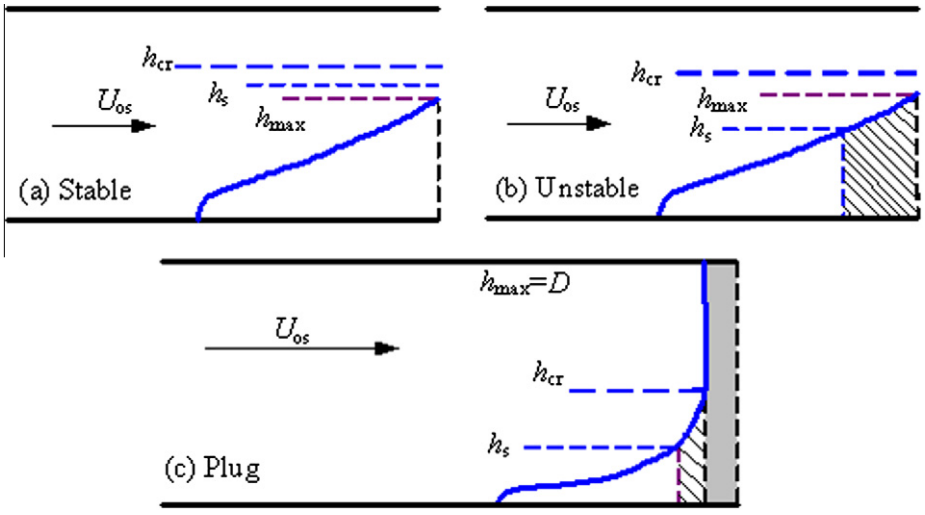

Fig. 9. Schematic description of the volume of water dragged upward (V_e): (a) $V_e = 0$; (b) V_e = dashed area; (c) V_e = dashed area plus the grey area.

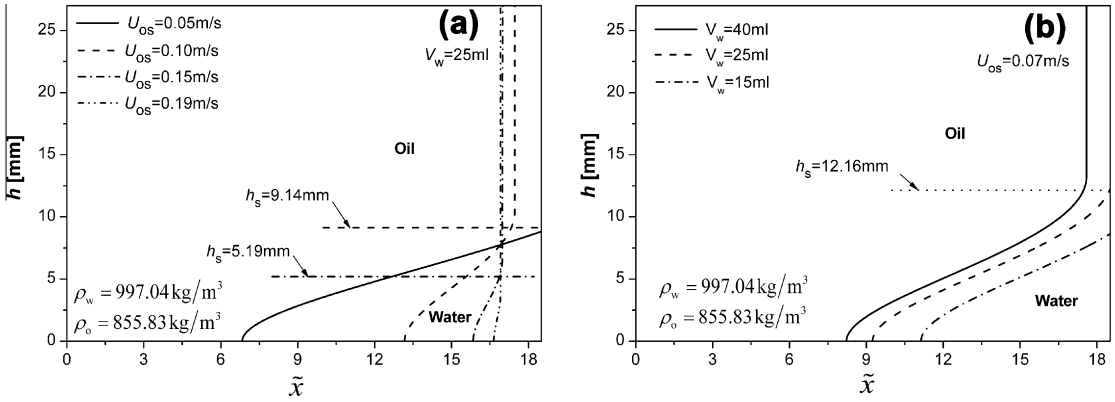

Fig. 10. Calculated water level profile for the $D = 27$ mm system.

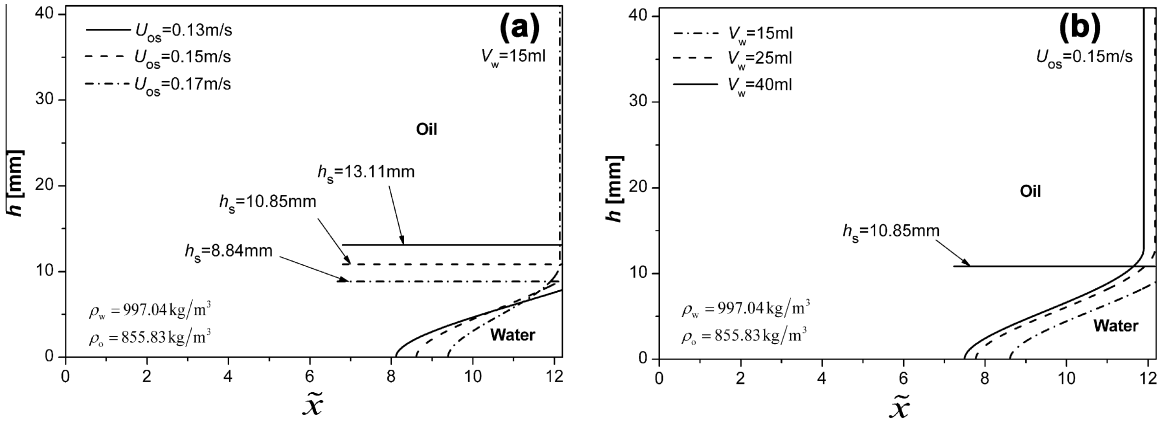

Fig. 11. Calculated water level profile for the $D = 41$ mm system.

Fig. 12. A picture of an eccentric elongated water drop taken in an upward inclined glass by-pass line (I.D.=15 mm, $V_w = 10$ ml).

4.2.2. Onset of water displacement

The calculated water level profile in the horizontal section is combined with the stability criterion of Eq. (1.1) with $C = 12$, $\beta = 0^\circ$ to determine the critical conditions for the onset of water displacement and the amount of water pushed into the upward inclined section. Obviously, the latter includes the water in the plug, once a plug is formed. However, it may include also water entrained from the waves formed in the unstable part of the plug tail. Assuming the water level profile is continuously rearranged according to Eq. (8), the amount of water displaced will include all the water corresponding to $h > h_s$. For a specified U_{os}, Eq. (1.1) is used to determine the minimal water level for the onset of interfacial instability, h_s. Obviously instability of the water interface ($h > h_s$) may result for lower U_{os} than that obtained when a constant (average) water level is considered (mechanism 1).

If the maximal water level, h_{max} is lower than h_s, the entire amount of water (V_w) remains in the horizontal section (Fig. 9a). The onset of water displacement corresponds to the conditions for which $h_{max} \geqslant h_s$. In view of the above, the maximal amount of water dragged into the upward section is assumed to be the water accumulated in the plug (if $L_2 > 0$) and in the part of its tail where $h > h_s$ (dashed zone in Fig. 9b and c), namely:

$$V_e = \int_{h_s}^{h_{cr}} \frac{A_w(h)}{dh/dx} dh + AL_2 \tag{17}$$

where dh/dx is given by Eq. (8). It is worth noting however, that the major part of the water displaced is from the plug formed ($V_e \approx A \cdot L_2$, see Fig. 13).

5. Results and discussion

The water level profile model and the stability analysis described in Section 4 were used to investigate water level profiles in the horizontal test section and the amount of water dragged into the upward test section by the laminar oil flow under the experimental conditions. Figs. 10 and 11 demonstrate the calculated water level profile in the horizontal section ($L = 0.5$ m) for the two pipes used in experiments $D = 27$ mm and $D = 41$ mm, corresponding to $\tilde{L} = L/D = 18.5$, 12.2, respectively ($\tilde{x} = x/D$ denotes dimensionless axial distance). The neutrally stable water level h_s is also indicated in the figures. According to the model described in Section 4.2.2, the water with $h > h_s$ may be dragged into the upward test section.

Figs. 10a and 11a show that upon increasing the oil flow rate, the water level rises more rapidly. For sufficiently high U_{os}, a water plug is formed, and its length increases with increasing U_{os} and the amount of water introduced into the system (V_w), resulting in larger amounts of water that can be dragged into the upward inclined arm. In a reasonable agreement with the experimental results, the model predicts that onset of water displacement is at $U_{os} = 0.08$, 0.07, 0.06 m/s for $V_w = 15$, 25, 40 ml in the $D = 27$ mm pipe, and at $U_{os} = 0.16$, 0.14, 0.13 m/s for $V_w = 15$, 25, 40 ml in the $D = 41$ mm pipe. Hence, higher oil flow rates are required to drag out the water in larger diameter tubes. For the same initial amount of water (but not the same holdup) the critical U_{os} is approximately proportional to D.

The water pushed into the upward section may be redistributed into an eccentric elongated drop, which due to gravity is situated near the bottom of the pipe. In order to substantiate this assumption, a transparent glass tube (I.D. 15 mm) was connected as a by-pass to the flow loop. The picture shown in Fig. 12 was taken in the 12° upward inclined glass by-pass for a case where 10 ml water was introduced into the by-pass loop and for a similar range of oil flow rates. At shallow upward inclinations, the water drop slowly crawls upward over the bottom of the pipe, with the largest upward velocity near the oil–water interface. Consequently, detection of water flow through any of the tapping valves is expected only after a certain period of time, depending on the downstream distance of the valve from the elbow. Indeed, the experimental results imply that the water velocity in the upward section is much lower than the oil superficial velocity, indicating that upon propagating upward, the water does not plug the oil flow.

A drift flux model is applied to represent the water drop rise velocity, whereby:

$$U_w = f(U_{os}) - U_{wB} = C_B U_{os} - U_{wB} \tag{18}$$

where U_{wB} is the water drop drift velocity in the lighter oil and C_B is the distribution coefficient, which is dependent on the water drop eccentricity.

Estimation of C_B and U_{wB} has been obtained based on the results shown in Fig. 4. As shown, a linear relationship results in a good fit considering the slope of the fit (the distribution coefficient) to be the same in the two systems ($C_B = 0.17$). The water propagation velocity can be represented by:

$$\begin{aligned} U_{w27} &= 0.17 \cdot U_{os} - 0.013 \\ U_{w41} &= 0.17 \cdot U_{os} - 0.015 \end{aligned} \tag{19}$$

With the above information on the water propagation velocity, the water withdrawal from the upstream tapping valves (during the measurement time, t of 5 min) can be calculated. The model predicts the amount of water that can be withdrawn from a tapping valve located at a distance l downstream the upward inclined arm provided the following three conditions are satisfied: $V_e > 0$, $U_w \geqslant 0$ and $t > l/U_w$, where V_e is the value obtained by Eq. (17). Figs. 2a–d and 3a–c show a comparison of the model prediction with the data of water withdrawal during 5 min from the $D = 27$ mm and $D = 41$ mm systems, respectively.

Fig. 2 shows that the model predictions for the system with diameter 27 mm are in a good agreement with the experiment data. In accordance with the experimental data, in the range of relatively low flow rates, water withdrawal from the upward inclined section may be zero although $V_e > 0$ is predicted, as the oil velocity is not large enough to overcome gravity and carry the water drop upward the inclined arm. However, for $V_e > 0$ and $U_w > 0$, larger U_{os} is required for the water to reach a tapping point located farther downstream during the measurement time of 5 min. At a sufficiently high oil flow rate, the entire amount of water introduced in the horizontal section can be withdrawn, provided the tap is open for a sufficiently long time. As shown in Fig. 3, the model predicts quite reasonably the experimental data also in the system with diameter 41 mm.

The results obtained imply that upon increasing the pipe diameter from 27 mm to 41 mm, the onset of water displacement is delayed to higher U_{os}. This is further reinforced by the results shown in Fig. 13, where the model predictions for the percent of water displaced (V_e/V_w) by the oil flow in these two pipes are compared for the same initial water holdup in the horizontal section (rather then the same total water amount). This figure also shows the results obtained when the displaced water include only the water in the plug ($V_e \approx A\,L_2$ in Eq. (17)). As can be observed, disregarding the amount of water entrained due to interfacial instability of the plug tail has a minor effect of the predicted results.

The effect of some variation in the oil physical properties due to changes in the operational temperature (5, 15, 25 °C) on the predicted amount of water displaced by the oil flow is shown in Fig. 14. Note that the variation in the water physical properties in this temperature range has a negligible effect on the results. The results show that the critical oil superficial velocity for the onset of water displacement decreases with increasing the oil viscosity and density (i.e., with lowering the density difference), and lower U_{os} values are required for displacing the amount of water trapped in the low section of the pipe. This is a result of the increased interfacial shear exerted by the more viscous oil. It may explain why higher viscosity crude oil pipelines are less susceptible to corrosion-products plugging of downstream equipments.

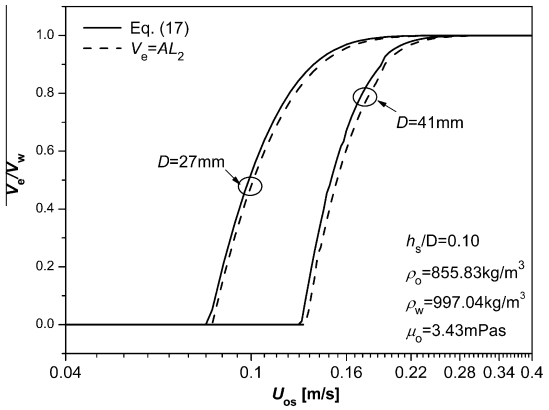

Fig. 13. Predicted V_e/V_w vs. U_{os} for the same water holdup in the two pipe diameter systems: solid line V_e according to Eq. (17), dashed line $V_e = A\,L_2$.

6. Up scaling to larger pipe diameters

Three mechanisms were considered for the onset of water displacement (Section 4): instability of the oil–water interface followed by water drop entrainment, the formation of water plug, and the formation of water-in-oil dispersion. From a practical point of view, a question may arise whether the mechanism for the onset of water displacement due to water plug formation (described in Section 4.2) is applicable to larger diameter pipes pertinent to the field-scale pipelines. In large diameter pipes the oil flow is turbulent and the mechanism of water breakage into drops and the formation of water-in-oil dispersion should also be considered.

The criterion for transition to dispersed flow (Brauner, 2001) suggests that transition to water-in-oil dispersion occurs when the turbulence in the continuous oil phase is sufficiently intense to break the dispersed water phase into droplets with a maximal diameter (d_{max}) smaller than a critical size of deformable/coalescing drops, d_{crit}. The minimal critical oil flow rate corresponds to dilute water dispersion, and is determined by applying the following criterion:

$$d_{max} \leqslant d_{crit} \tag{20}$$

with:

$$\tilde{d}_{max} = 0.55\left(\frac{\rho_o U_{os}^2 D}{\sigma}\right)^{-0.6} f_o^{-0.4} \tag{21.1}$$

$$\tilde{d}_{crit} = \mathrm{Min}(\tilde{d}_{c\sigma}, \tilde{d}_{cb}) \tag{21.2}$$

$$\tilde{d}_{c\sigma} = \sqrt{\frac{0.4\sigma}{|\Delta\rho| g \cos\beta' D^2}}, \quad \beta' = \begin{cases} |\beta|, |\beta| < 45^\circ \\ 90^\circ - |\beta|, |\beta| > 45^\circ \end{cases} \tag{21.3}$$

$$\tilde{d}_{cb} = \frac{3}{8}\frac{\rho_o}{|\Delta\rho|}\frac{f U_{os}^2}{Dg\cos\beta} \tag{21.4}$$

where σ is the interfacial tension and f_o is the friction factor of the oil phase. Considering rough pipes, the following equation is used (Haland, 1983):

$$f_o = \left[-3.6\log_{10}\left(\frac{6.9}{Re_o} + \left(\frac{k_s}{3.7D}\right)^{1.11}\right)\right]^{-2} \tag{22}$$

where k_s denotes the roughness scale. Note that in rough pipes, this friction factor model replaces also Eq. (10). Pipes with $D < 0.1$ m are galvanized steel pipes with $k_s = 0.15$ mm, while larger pipes are considered as commercial steel pipes with $k_s = 0.045$ mm (http://www.efunda.com/formulae/fluids/roughness.cfm).

The effect of the pipe diameter on the critical oil superficial velocity and the corresponding critical oil Reynolds number predicted by the three mechanisms considered with water holdup corresponding to $h_w/D = 0.05$ is shown in Fig. 15. All three mechanisms predict an increase of the critical oil superficial velocity with increasing the pipe diameter. In all cases the water plug mechanism yields the lowest critical oil flow rate for the onset of water displacement. Hence, it is plausible that it can be considered as the dominating mechanism also when up-scaling to larger diameter pipes encountered in field operations. For pipe diameter larger than about 0.05 m, the critical oil velocity for plug formation corresponds to turbulent oil flow, hence the pipe roughness scale has to be considered in the modeling. However, the effect of the pipe roughness is very mild. Assuming a smooth pipe would increase the predicted critical oil flow rate by less than 1%. Note that in the turbulent regime the critical U_{os} is proportional to D^n, where $n \approx 0.5$ for water plug formation and oil–water interface instability. For water-in-oil dispersion mechanism, $n = 0.24$ and $n = 0.43$

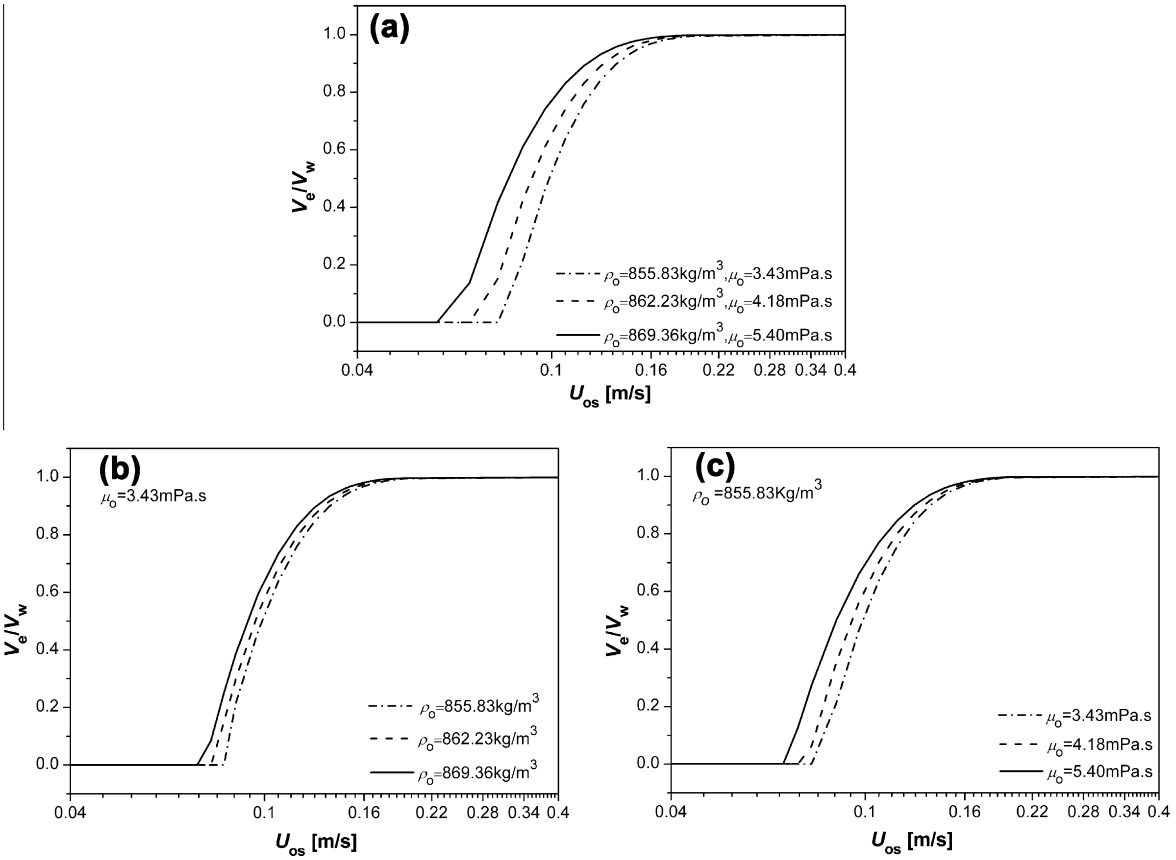

Fig. 14. The effect of oil physical properties on the volume of water withdrawn (V_e) with V_w = 15 ml, D = 27 mm: (a) different oil density and viscosity; (b) different oil density; (c) different oil viscosity.

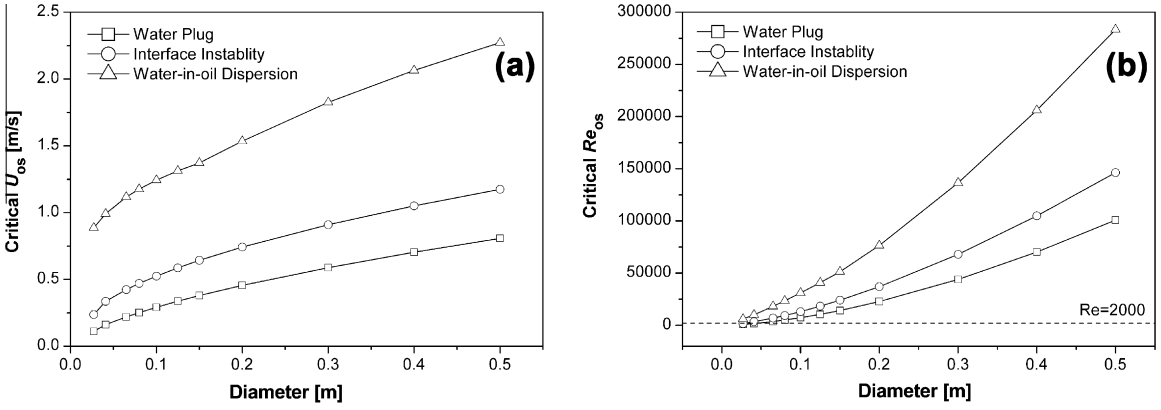

Fig. 15. The critical oil superficial velocity and Reynolds number according to the three possible mechanisms for initial water level of h_w/D = 0.05.

(for D < 0.2 m and D > 0.2 m, respectively for the properties of the studied oil–water system). The models used indicate that the critical oil superficial velocity for water plug formation and oil–water interface instability decreases with increasing water holdup in the horizontal section, while the minimal critical U_{os} for the formation of water-in-oil dispersion (3rd mechanism) is independent of the water holdup. Hence, the plug formation is predicted to be the dominant mechanisms also for higher water holdups.

7. Conclusions

Stemming from blockage incidents of the oil products pipelines happening many times in China, an experimental study and a theoretical analysis have been conducted for investigating the characteristics of water displacement by oil flow. The experiments were conducted in two flow loops with pipe diameters of 27 mm and 41 mm consisting of downward inclined, horizontal and upward inclined sections. Water withdrawal from different tapping valves placed on the upward test section was measured.

A model for predicting the water displacement by the oil flow is suggested. The model is based on the formation of a water plug in the lowest elbow (i.e., the horizontal section), which is pushed by the oil flow into the upward inclined arm. The predicted amounts of water withdrawn from the tapping valves favorably compare with the experimental results obtained for the two different pipe diameters. The model also predicts that water displacement is

facilitated by increasing the oil viscosity (and density). In natural gas pipelines, water displacement by gas flow would require much higher critical superficial velocity of the carrying gas.

Two other competing mechanisms for the onset of water displacement by the oil flow were considered: instability of the oil–water interface in the horizontal section (followed by drop entrainment), or the formation of water-in-oil dispersion. These two mechanisms largely over predict the experimental critical oil flow rates in the two pipes. Up-scaling to larger pipe diameters is also considered. The analysis indicates that water plug formation is the dominating mechanism for water displacement also in large diameter pipes encountered in field operation.

Further validation and improvement of the model require visualization of the flow pattern and direct measurements of the water velocity and holdup. These measurements were not possible in the present stainless steal test section. Future work includes a construction of a new experimental setup with a transparent pipe to overcome these limitations.

Acknowledgement

The first author was supported by the China Scholarship Council.

References

Arirachakaran, S., Oglesby, K.D., et al., 1989. An analysis of oil–water flow phenomena in horizontal pipe. In: SPE18836, pp. 155–167.

Brauner, N., 1998. Liquid–liquid two phase flow. Heat Exchanger Des. Update 5 (1) (Chap.2.3.5).

Brauner, N., 2003. Liquid–liquid two-phase flow systems. In: Bertola, V. (Ed.), Modeling and Experimentation in Two-phase Flow Phenomena. Springer-Verlag (CISM Udine).

Brauner, N., Moalem Maron, D., 1992. Stability analysis of stratified liquid–liquid flow. Int. J. Multiphase Flow 18, 103–121.

Brauner, N., Moalem Maron, D., 1989. Two-phase liquid–liquid stratified flow. Physico-Chem. Hydrodyn. 11, 487–506.

Brauner, N., 2001. The prediction of dispersed flows boundaries in liquid–liquid and gas–liquid systems. Int. J. Multiphase Flow 27, 885–910.

Chakrabarti, D.P., Das, G., et al., 2007. Identification of stratified liquid–liquid flow through horizontal pipes by a non-intrusive optical probe. Chem. Eng. Sci. 62, 1861–1876.

Chen, J., Yu, D., et al., 2001. An experimental investigation on the pressure drop of oil–water two-phase flow in horizontal pipe. J. Exp. Mech. 16, 402–408.

Chen, J., Yu, D., et al., 2003. Study on pattern transition of oil–water pipe flow. J. Hydrodyn. A18, 355–364.

Haland, S.E., 1983. Simple and explicit formulas for the friction factor in turbulent pipe flow. J. Fluids Eng. 105, 89–90.

Lovick, J., Angeli, P., 2004. Experimental studies on the dual continuous flow pattern in oil–water flows. Int. J. Multiphase Flow 30, 139–157.

Rodriguez, O.M.H., Oliemans, R.V.A., 2006. Experimental study on oil–water flow in horizontal and slightly inclined pipes. Int. J. Multiphase Flow 32, 323–343.

Shi, H., Jepson, W.P., et al., 2003. Segregated modeling of oil–water flows. In: SPE84232, pp. 1–10.

Tao, J.H., Tian, Y.L., et al., 2006. Analysis of operational problem and the solution in the products pipeline. Oil Gas Storage Transport. 25, 59–61.

Yang, Q.Y., 2009. The Analysis and Solution to the Cause of Sediments for Lan–Cheng–Yu Products Pipeline. M.Sc. Thesis, Faculty of Oil & Gas Storage and Transportation. China University of Petroleum, Qingdao, China.